Chapter 6

Flexible MEMS Technology and Shear Stress Sensor Skin

6.1 Introduction

In some research involving the study and control of a distributed system, it is essential to obtain the real-time profiling of certain physical parameters such as temperature, force, pressure or shear stress on a 3-D object. If the surface of the object is flat, the profiling can be achieved by using a monolithic MEMS sensor array [1]. However, this can be much more difficult if the surface is non-planar. For example, in aerodynamics study, the most popular research objects such as an air foil have non-planar or even high-curvature surfaces. In the past, when real-time distribution measurement was necessary, embedding all the discrete sensors on a surface was the only way. Nevertheless, large sensor size and difficulty in packaging, i.e., plumbing and wiring, have limited the wide application of these measurements.

It has been our goal to develop a flexible MEMS technology to produce smart skins (with integrated MEMS devices) that can be easily taped or glued on non-planar surfaces. Retrospectively, Barth et al. [2] in 1985 reported the first version of this idea with a one-dimensional flexible Si-diode temperature sensor array in which a polyimide strip was the flexible material connecting Si islands formed by isotropic HNA etching. However, the authors claimed that this technology needed some major improvements before it could be applied to more sophisticated sensor systems. This sensor skin concept, unfortunately, was not pursued further until 1994, when Beebe and Denton [3] presented their effort on improving the robustness and reliability of flexible polyimide skins. Their skins did not

bear any real devices. The major lead failure mechanism was identified as the breakage of the thin silicon on the island periphery (Figure 6.1). Since the basic process was the same as that developed by Barth, the methods used to enhance the robustness, including taping and coating of epoxy on both front and back sides of the skins, were all performed manually as post-processing steps. It is obvious that these are not the ideal solutions for a reliable as well as mass-producible smart skin technology. Recently, we learned that, almost concurrent to our effort, Bang and Pan [4] also have an on-going project to develop a flexible heat-flux sensor array which is made by direct deposition of thin-film metals on commercial Kapton polyimide substrates, based on the smart skin technology reported by Mehregany et al. [5]. As a matter of fact, this basic technology is nothing new and has already been used to make polyimide-based hot-film shear stress sensors [6,7,8,9,10,11]. A large array of metal temperature sensors can be made in this way, but its drawback is that neither ICs nor silicon MEMS can be integrated with this approach; hence, only limited types of sensors are available and hybrid assembly of electronic circuits is unavoidable.

In comparison, the work we present here is a new flexible skin technology designed to be compatible with both IC and MEMS fabrications. Due to the much stronger periphery of the silicon islands formed by nearly vertical RIE, the skin reliability has been greatly improved. Moreover, we have realized a 2-D flexible skin integrated with more than 100 shear stress sensors. This skin has further been mounted on a 3-D leading edge of a delta wing and successful 2-D shear stress measurements are obtained. For the first time, the air flow boundary layer separation over the leading edge of a delta wing is determined experimentally in real time.

6.2 Flexible Skin Technology

As mentioned in the previous section, almost all the lead failures on the flexible skins made by Barth and Beebe were caused by the breakage of the thin peripheries on the Si island during the squeezing and folding test. The thin and weak Si island periphery was

the natural result of isotropic HNA etching (Figure 6.1a). In comparison, the island shapes formed by caustic anistropic etchants such as TMAH or KOH and by the combination of anisotropic etching and RIE are much more robust when subjected to squeezing and folding (Figure 6.1b & c). Unfortunately, the above caustic etchants attack all types of polyimides, so that polyimide layers must be coated after the islands are formed or protected from the etchants during the etching. Using gold or other expensive metals as the protection materials is not only costly, but also incompatible with IC processes. The one-sided etching apparatus is not usable as the pressure difference between the two sides would cause the rupture of the polyimide near the end of the etching, or a small leak on the wafer near the end of the etching would attack the polyimide on the front side. The approach of coating polyimide after island formation is not feasible either, unless proper material remains to support the islands after the etching and can be removed with ease after the polyimide is coated. Our new flexible MEMS technology is based on this idea with additional modifications.

Figure 6.2 is the simplified process flow of this new technology. It starts with selective TMAH or KOH etching on the backside of a double-side polished (100) Si wafer with silicon nitride being the mask material to form a Si membrane of desired thickness. Aluminum is evaporated on the front side and patterned to cover the area between future Si islands. Polyimide is spun-on, cured and patterned to cover the patterned Al completely. Normal Al metallization then follows to provide electrical leads. Another polyimide layer is spun-on and patterned to expose the bonding pads. RIE etching on the backside using Al as masking material removes the Si on the streets between Si islands. Here the first layer of Al serves as the etch stop during this SF_6-based RIE etching step. Finally, a thick polyimide layer is spun-on and cured on the backside to sandwich the Si islands. The finished skins are then cut off from the Si wafer frame by a razor blade.

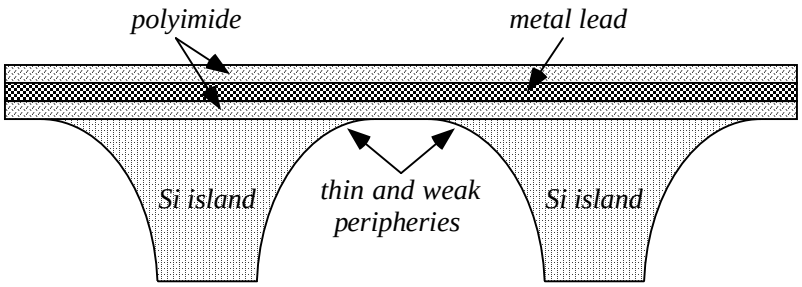

(a) by HNA isotropic etching.

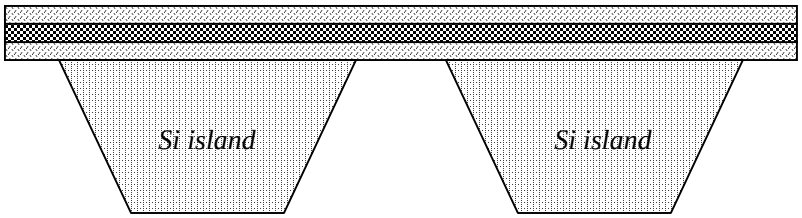

(b) by anisotropic etching (TMAH or KOH).

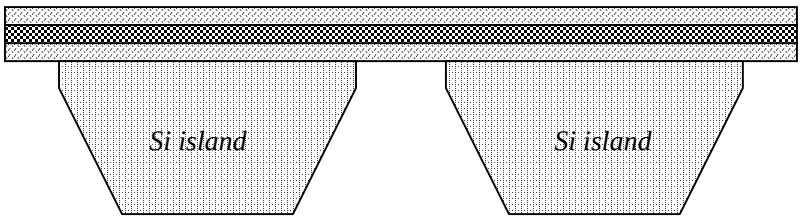

(c) by a combination of anisotropic etching and RIE.

Figure 6.1 Si island shapes formed by different ways.

Figure 6.3 shows the photograph of a fabricated flexible skin about 8 cm in diameter with 2 x 2 mm^2 Si islands. Since we are only demonstrating the concept here, the skin did not contain actual devices. However, it is obvious that the above process is compatible with IC process as it involves only aluminum and polyimide which are commonly used in IC fabrication. We can start with a wafer with fabricated IC and MEMS (without metallization) and the above process needs only minimal adjustment to produce flexible MEMS skins. Such flexible MEMS skins have already been realized and will be presented in the next section.

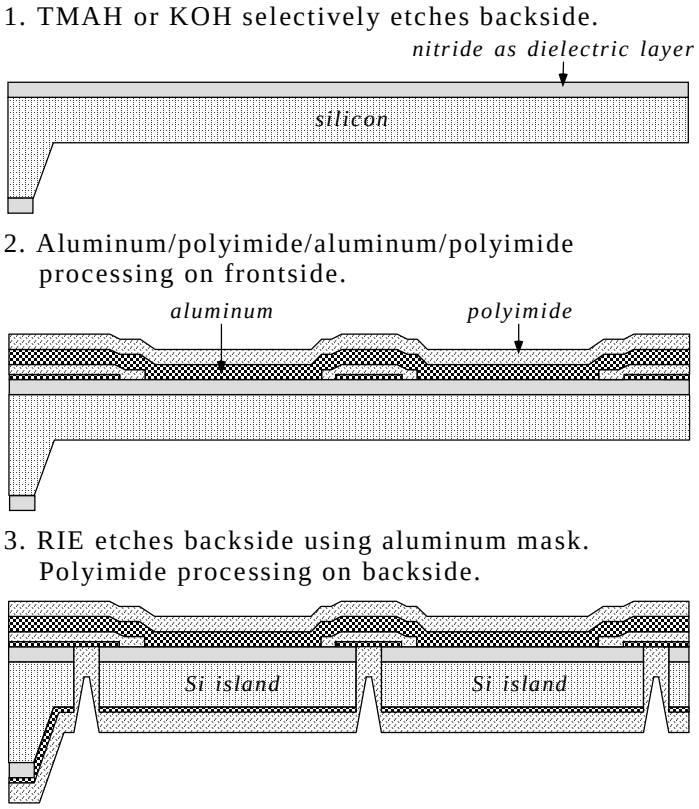

Figure 6.2 Simplified process flow of the new flexible skin technology.

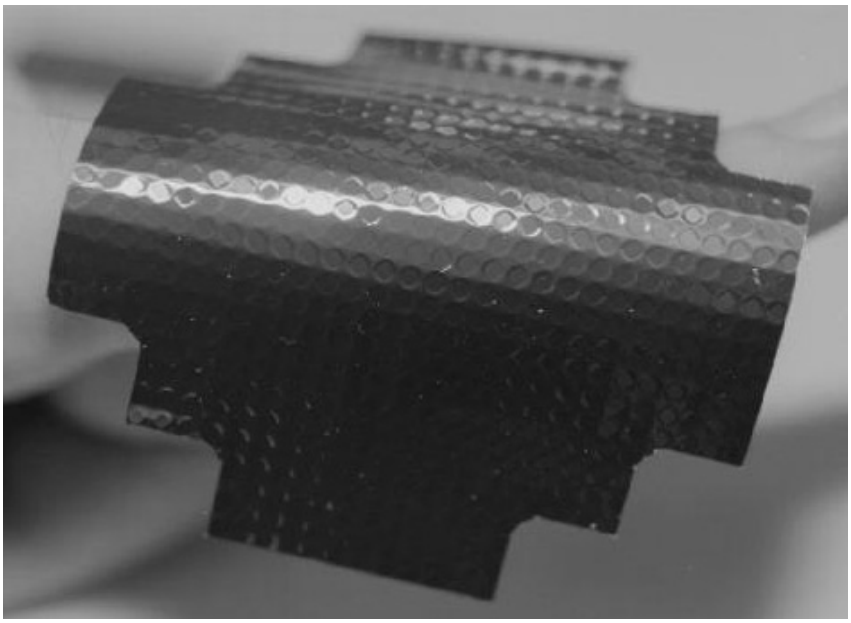

Figure 6.3 Picture of a wafer-size flexible skin.

In the above process, the Si islands are formed by RIE-etching the Si diaphragm. Since the diaphragm thickness is less than 100 μm and the RIE etching is nearly vertical, we can well-define islands with dimension as small as 100 μm and spacing less than 50 μm, which makes it possible for the skin to be applied on a very high-curvature surface with good conformal coverage. For obvious reasons this can not happen if any of the island-forming techniques shown in Figure 6.1 are used (HNA etching is isotropic and TMAH or KOH etching requires large corner compensation structures to avoid fast undercut of corners). Of course, there is some disadvantages in using Si diaphragm and thin islands. First, extreme care must be taken of the wafers during processing as they are very fragile. However, if the individual skin is not too big, the wafers are reasonably robust to survive the whole process. Moreover, if a robust one-sided wet Si etching or deep RIE etching is available, the formation of Si diaphragm can be delayed until all the processing steps on the wafer front side are finished, thus reducing the risk of wafer breakage significantly. Second, thin Si islands can not take as much force as thick ones. This is generally not a concern for most applications where the skins do not contact other objects after being mounted.

Table 6.1 Properties of DuPont Pyralin® PI-2808 polyimide.

Density	2.3 g/cm^2
Tensile strength	210 MPa
Young's modulus	2.3 GPa
Elongation at break	88%
Stress for 10 μm thick film	18 MPa
Peel test adhesion	0.23 g/mm
Dielectric constant	3.3
Cure temperature	350 °C
Decomposition temperature	580 °C

Polyimide was chosen as flexible skin material, just as in the previous works due to

its good mechanical strength and flexibility. We used DuPont's Pyralin® PI-2808 polyimide which has a tensile strength of 210 MPa [12]. This value is one of the highest among all the spin-coated polyimides and is almost the same as that of Kapton (231 MPa) [13], a product also made by DuPont and commonly used as a flexible runner for providing reliable connections to moving print heads. Some properties of the PI-2808 polyimide are listed in Table 6.1.

In the process, the thickness of each polyimide layer on the front side of the wafer is 3-4 μm after curing at 350°C. Since the polyimide layers are not exposed to strong acids or bases, their mechanical properties are not degraded. Then a total of 7 μm thick polyimide on the front should be able to stand a tensile force of 1.47 kg/mm, which is fairly strong. However, the peel-off forces of the polyimide from Si substrates given by the manufacturer is only about 0.23 g/mm. Therefore, even a very small shear force exerted on a Si island would peel it off. One solution to this problem is to spin thick polyimide (10 μm) on the back side of the wafer to fully encapsulate the islands. The total polyimide thickness between islands becomes 17 μm and the maximum tensile force that the skin can stand is increased to 3.57 kg/mm.

As for the metal leads, they are completely embedded in two polyimide layers on the flexible area. Also, the Si islands they are sitting on do not have weak edges. Therefore, they should be able to stand repetitive squeezing and bending without breakage. In our initial testing, no metal lead failure has been observed after more than 100 times of 90°-180° bending.

6.3 Flexible Shear Stress Sensor Array

It is important to demonstrate that useful MEMS devices can indeed be integrated on a flexible substrate with this flexible skin technology. Based on the following two considerations, we target our first effort on the development of a flexible shear stress sensor array. First, the micromachined thermal shear stress sensor we developed previously has been useful in turbulent flow study since its invention. For example, arrays

of shear stress sensor on a rigid substrate have been used to detect the real-time shear stress distribution on a flat (i.e., 2-D) surface for flow-induced drag reduction study [1,14]. However, its application has so far been limited to 2-D flow due to the lack of flexible packages. The development of a flexible shear stress sensor array is the only way to extend its application to 3-D flow. Second, the fabrication of shear stress sensors is a surface micromachining process with reasonably high complexity. It will be a good demonstration of the compatibility between the flexible skin and MEMS technologies.

Figure 6.4 shows the simplified fabrication process flow with cross-sections of the flexible shear stress sensor array. The detailed process description is in Appendix A. It is basically the combined fabrication processes for the shear stress sensor and the skin. The only mixing is that contact holes are opened after the first aluminum/polyimide processing so that they are fresh and clean for the immediately following metallization. High-quality double-side polished (100) Si wafers and good double-side alignment marks made at the very beginning of the fabrication are crucial to this complicated process. Figure 6.5 and Figure 6.6 are the photographs of a shear stress sensor and the finished flexible sensor respectively. The skin is 1 cm wide, 3 cm long, and it consists of two 32-sensor rows with a horizontal pitch of 635 μm and many other test devices (a total of more than 100 sensors). The two sensor rows are 5 mm apart and located between the pairs of white square boxes in the picture. Their bonding pads are extended to the left and right edges of the skin. The layout is designed in such a way that each sensor row spans the semi-cylindrical surface (1.3 cm in diameter) of a delta wing leading edge under study with an angular resolution of 5.6^{o}. Each sensor occupies 250 x 250 μm^2 and the dimension of each Si island is 450 μm x 550 μm (75 μm thick) to fully accommodate one sensor and to achieve excellent surface smoothness and conformability. Fig. 7 shows the picture of a skin sitting on a conic object. Its good flexibility is seen from the bending of the skin due to gravitation.

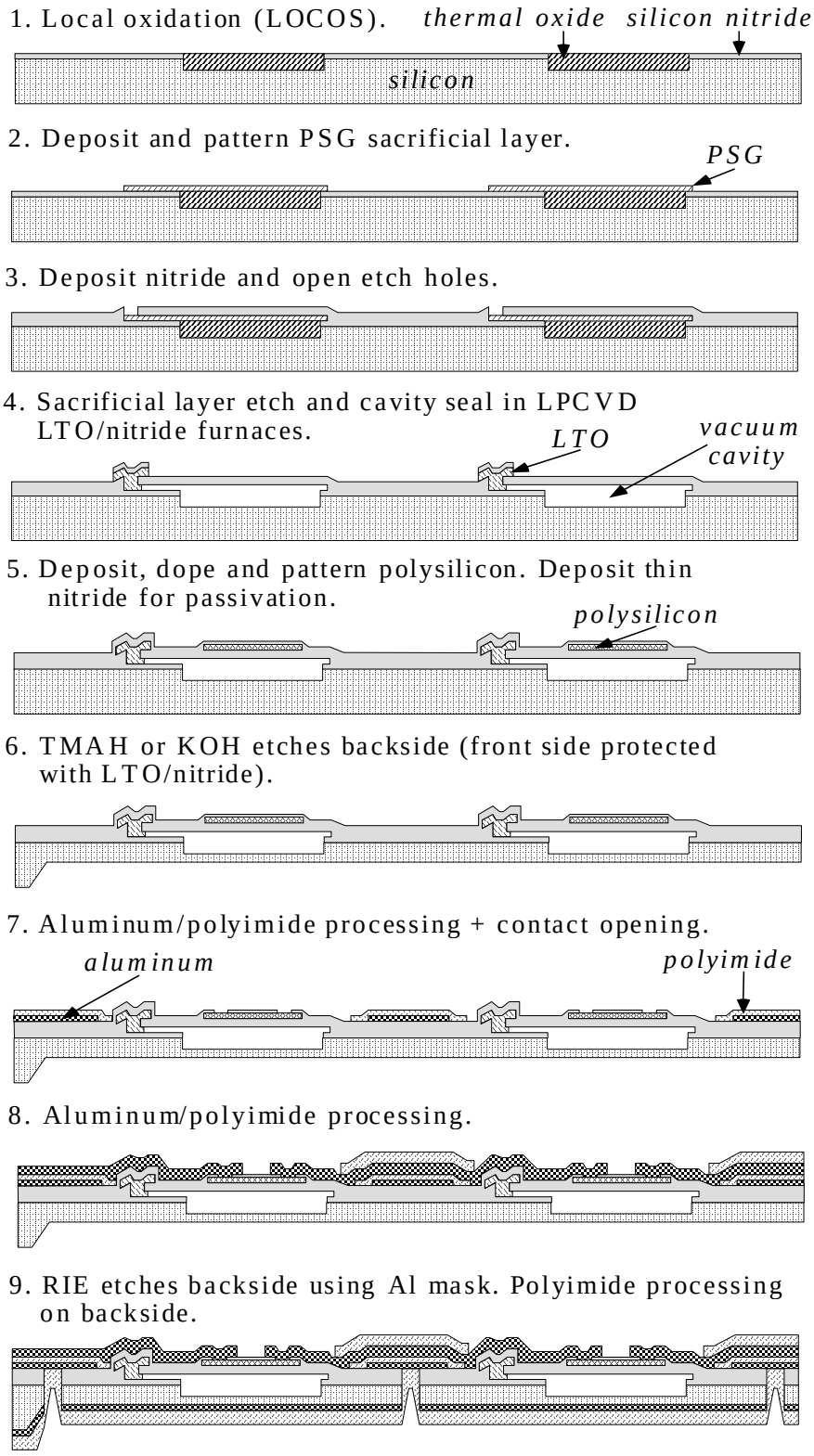

Figure 6.4 Fabrication process flow of the flexible shear stress sensor skin.

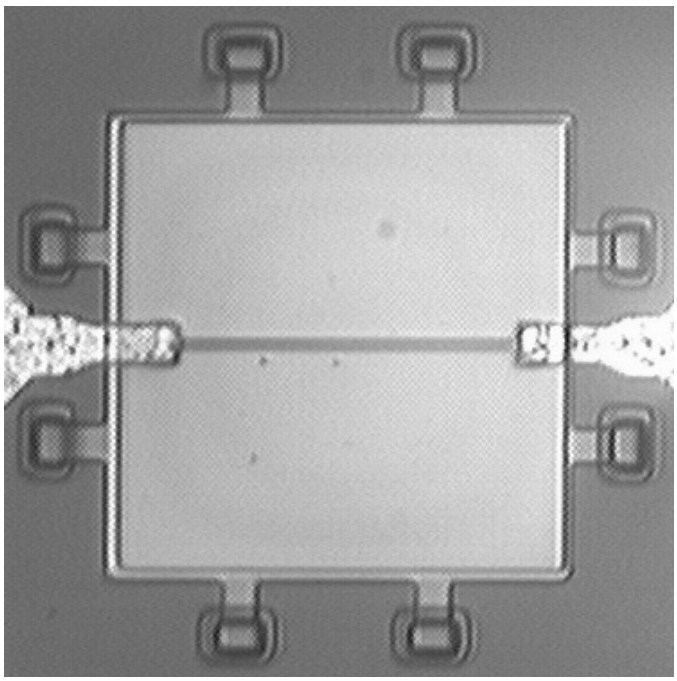

Figure 6.5 Photograph of a shear stress sensor. A square silicon nitride diaphragm (200×200 μm^2) with an embedded polysilicon wire is on top of a vacuum-sealed cavity.

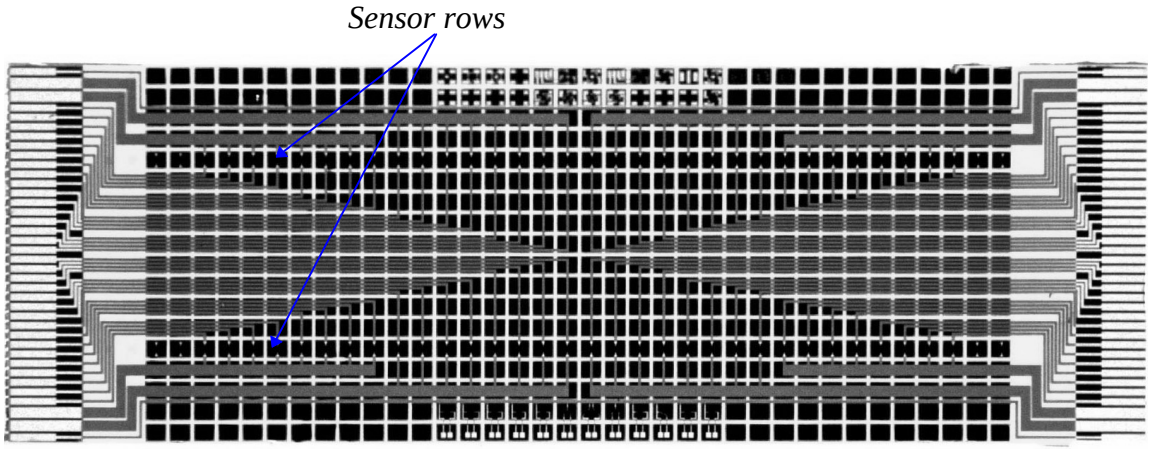

Figure 6.6 Picture of a flexible shear stress sensor array (1 cm × 3 cm).

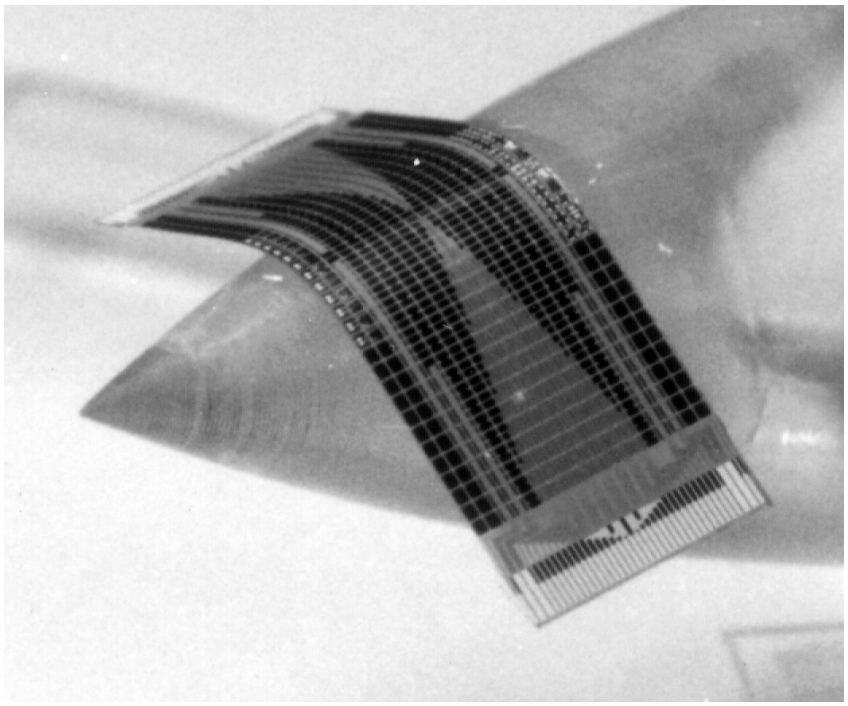

Figure 6.7 A flexible shear stress sensor skin sits on a conic object. The bending is caused by gravitation.

6.4 Packaging and Calibration of the Shear Stress Sensor Skin

The shear stress sensor skin is specially designed for the shear stress measurement on the leading edges of the delta-wing model in the UCLA Fluid Mechanics Laboratory, which is shown in Figure 6.8. It has a swept angle of 56.5^{o}. The leading edges span 36.5 cm from the apex to the trailing edge. Their surfaces are semi-cylindrical with a diameter of 1.3 cm. For the testing purpose, the leading edges are detachable and one of them is further divided into many blocks of removable semi-cylinders 2 cm long and 1.3 cm in diameter. The block on which the sensor skins will be mounted is recessed by about 100 μm to compensate the skin thickness. By moving the skin block along the whole leading edge block by block, we are able to map out the steady-state shear stress distribution, which is enough in laboratory testing. Of course, if instantaneous shear stress profiling is required, the whole leading edge surface has to be covered with sensor skins. This will be difficult, if not impossible, because of the huge amount of external leads and

electronics involved. The best solution will be the integration of sensors with electronics, as we will discuss later in this chapter.

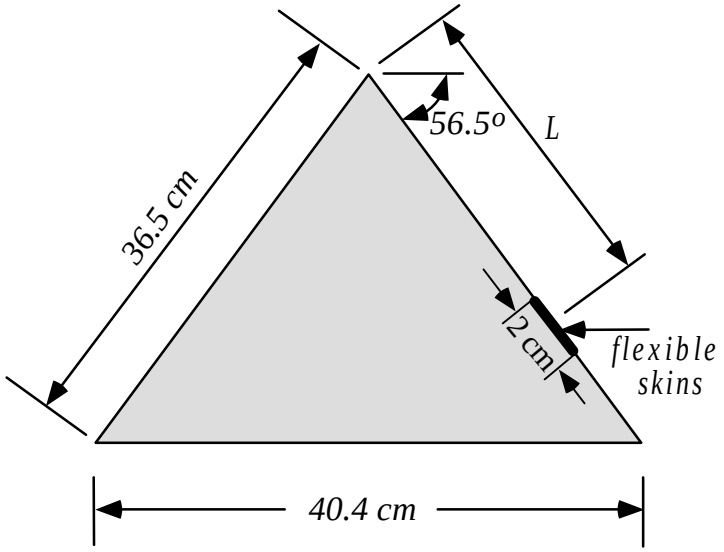

Figure 6.8 Schematic of the delta wing.

Figure 6.9 shows the schematic of the cross section of the packaged skin block. The packaging procedures are as follows: first, two skins are glued to the semi-cylinder with the sensors on the curved surface and the bonding pads extended to the flat surface; then a circuit board with pre-soldered wires is attached to the flat surface next to the bonding pads of the skins; ultrasonic wire bonding is performed to electrically connect the sensor leads on the skin to the circuit board; finally the bonding wires are fixed by epoxy. Here, the circuit board is a piece of Si with gold bonding and soldering pads specially designed and fabricated for this purpose (Figure 6.10). The finished block is then shown in Figure 6.11, which is ready for delta wing testing.

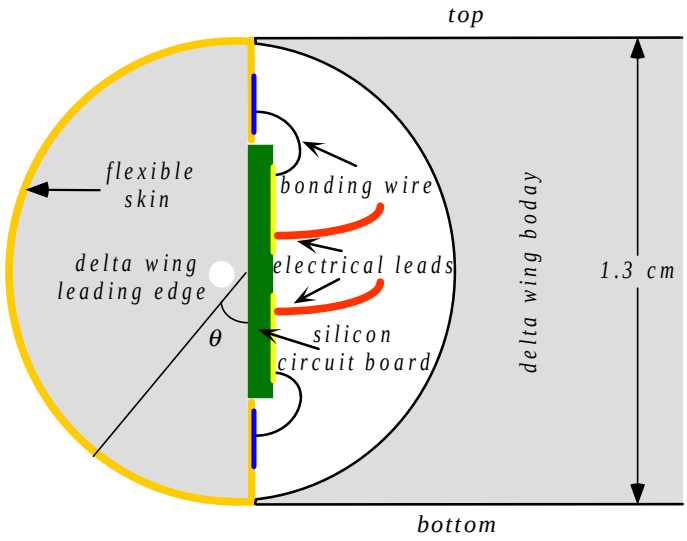

Figure 6.9 Packaging scheme for the flexible shear stress sensor skin on delta wing leading edge block.

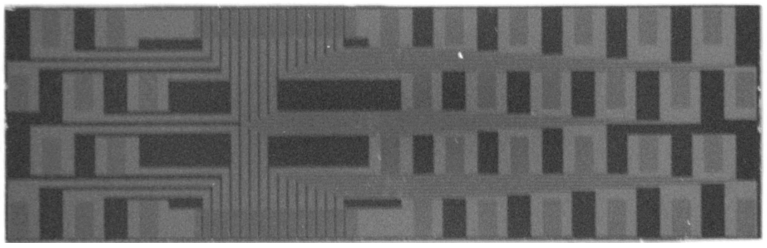

Figure 6.10 Picture of a Si circuit board.

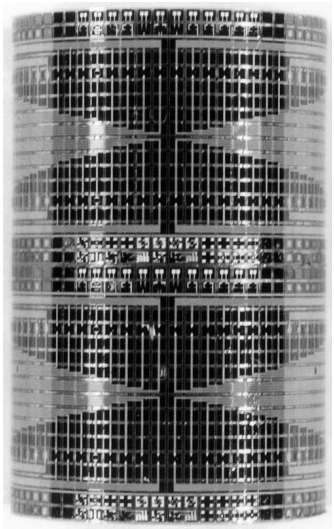

Figure 6.11 Two flexible skins wrapped around on a semi-cylindrical block, 2 cm long and 1.3 cm in diameter.

Before the packaged skin block is mounted on the delta wing for shear stress distribution measurement, it is calibrated by using the flow-over-cylinder method. The skin block and the other dummy blocks are combined together to form a long semi-cylinder. Another piece of semi-cylinder with the same length is attached to the long semi-cylinder to form a full cylinder, which is placed inside the wind tunnel with the skin surface facing the flow. The sensor outputs at different flow velocities are measured by using an A/D converter. Since the shear stresses at different ϕ on the middle section of the cylinder can be calculated from the flow velocity, the sensors are calibrated. These calibration results agree well with those obtained in a fully developed 2-D channel flow where a skin is flushed mounted on the wind-tunnel wall (Figure 6.12). We can conclude that the sensors on the flexible skin behave the same as those on rigid substrates because the square of the output voltage is proportional to the one-third power of shear stress τ with a sensitivity of 100 mV/Pa under constant temperature bias.

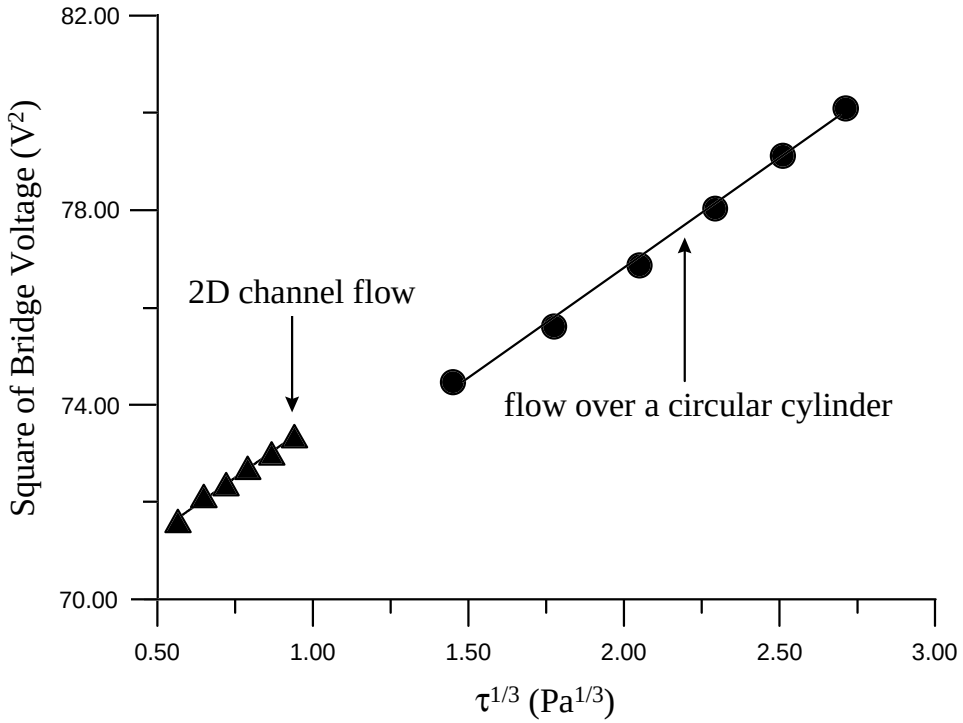

Figure 6.12 Calibration results of the sensors on flexible skins.

Another interesting result obtained from the flow-over-cylinder calibration method is the detection of flow separation by the sensor skin. In Figure 6.13, the local shear stress has a minima at $\phi \approx 85^{o}$, which is corresponding to the flow separation point in the 2-D flow field. This value is very close to that reported by other researchers [15,16].

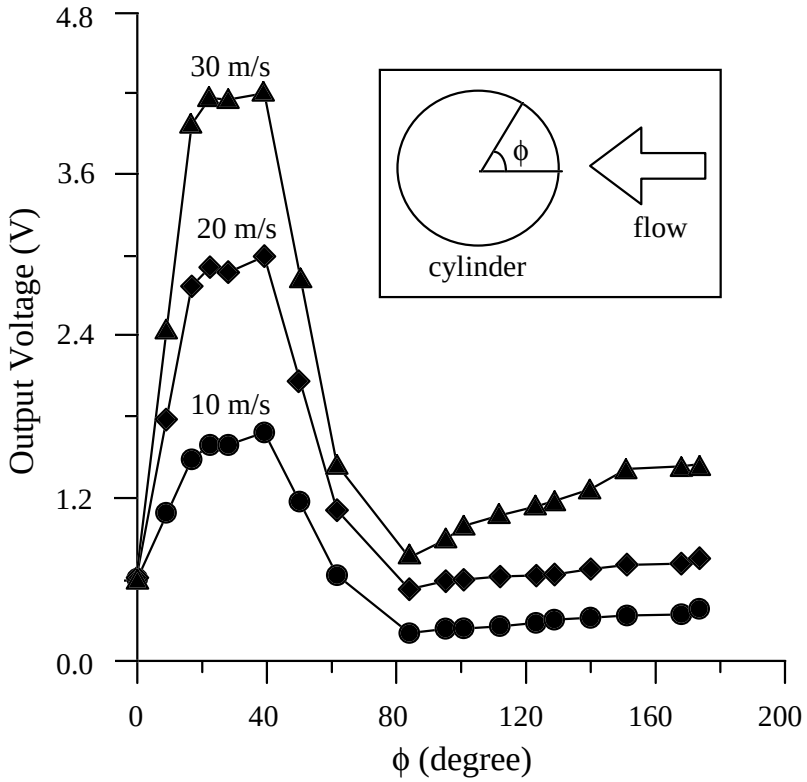

Figure 6.13 Flow separation at $\phi \approx 85^{o}$ on a cylinder is detected during the calibration.

6.5 Measurement on Delta Wing

The operation of a delta-wing at certain angle of attack depends on the counter-rotating leading edge vortex pair, as shown in Figure 6.14. Recently, there have been some studies on manipulating the vortex patterns to achieve better stability and maneuvrability at high angle of attack. The control scheme developed by the UCLA-Caltech research group is to selectively activate millimeter-size micro-flaps on the leading edge curvature. It has been experimentally confirmed that the control is most effective when the flaps just before the flow separation line are deflected out of plane

[17,18]. Therefore, the correct measurement of the flow separation line along the leading edge surface is essential to the success of this control scheme.

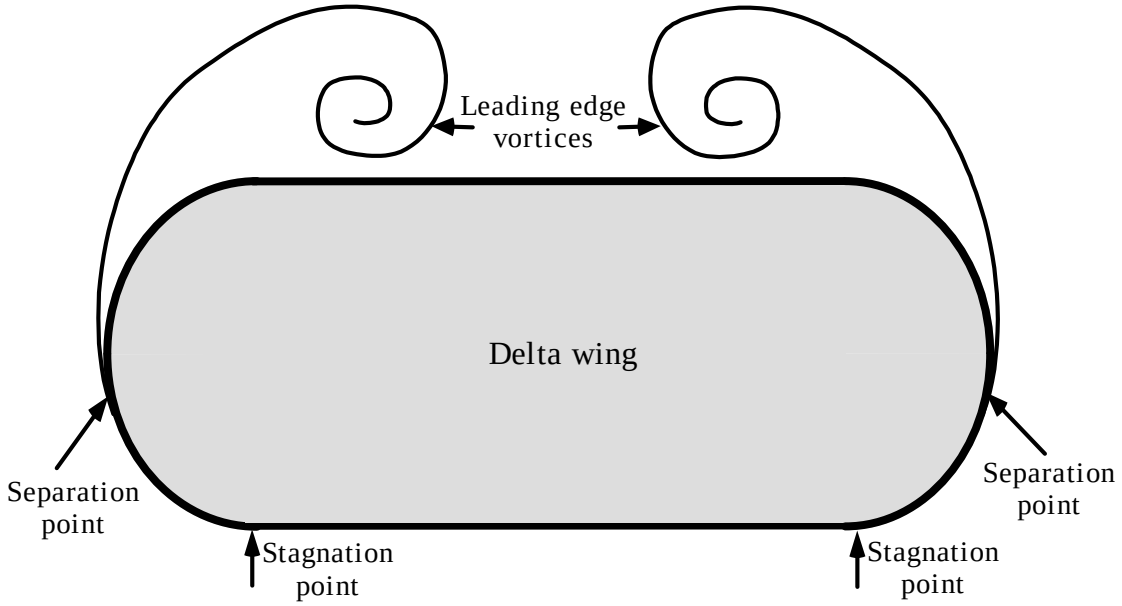

Figure 6.14 Flow separation on the leading edges of a delta wing.

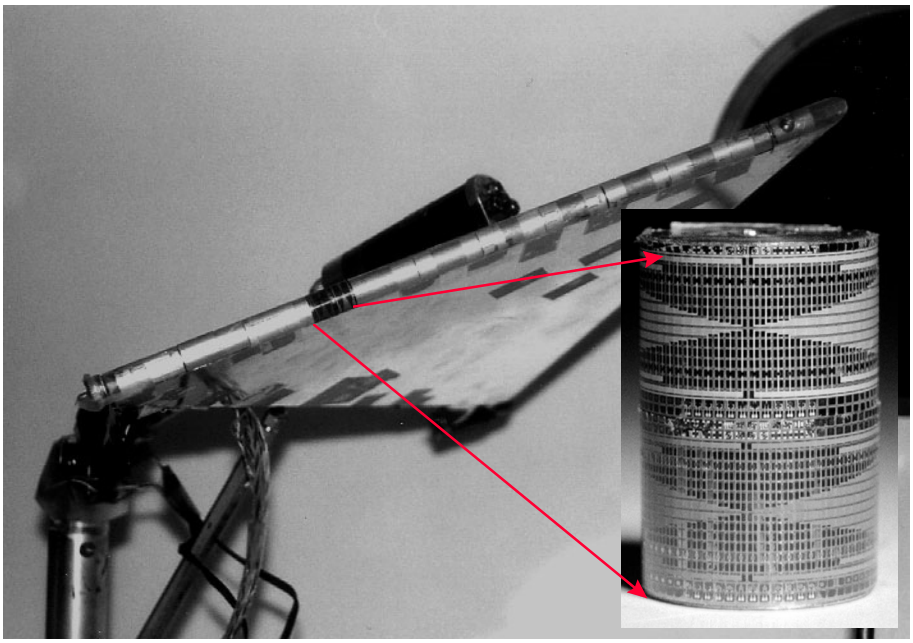

Figure 6.15 Picture of the skin-mounted delta wing model.

The test section of the wind-tunnel used for this study is 22 ft (6.7 m) long with a cross-sectional area of 3 ft by 3 ft or 0.9×0.9 m^2. The maximum air flow speed is 45 m/s. Figure 6.15 shows the delta wing model together with the mounted flexible skins installed in the wind-tunnel. The Reynolds number can be calculated by using the chord length of the delta wing, i.e., the distance from the apex to the middle of the trailing edge, as the characteristic length l. It is about 5.4×10^5 at an air flow speed of 30 m/s.

Measurements have been done for different flow velocities (U), skin locations (L) and angles of attack (AOA, defined as the angle between the air flow and the delta wing plane). For example, Figure 6.16 shows the averaged output voltages (after gain of 10) of the sensors for U = 30 m/s, L = 29 cm and $AOA = 30^o$. Sensor locations are indicated by θ, which is 0° at the bottom surface and 180° at the top surface. The averaged shear stress has a minima at about 110^o. Here, we can not assume that the flow boundary layer starts to separate from the leading edge surface at this location because the 3-D flow field is much more complicated than the flow over a cylinder. Fortunately, there is another unique phenomenon related to the flow separation, that is, the surface shear stress fluctuation stays low before separation, and rises sharply after separation (Figure 6.17). Therefore, we can identify a separation point through the measurement of the root-mean-square (RMS) value of shear stress fluctuation. Figure 6.18 shows the RMS results of one measurement, from which the separation point is found to be at $\theta = 80^o$. In fact, this is the first time separation points are experimentally determined in real time. The separation line along the leading edge is consistent with the data measured from a single shear stress sensor that was placed around the leading edge point by point in steady state flow (Figure 6.19) [19]. Based on our data, it is concluded that, for real time flow control, a single sensor is no longer enough and the flexible shear stress arrays are necessary because the flow separation point along the leading edge is a function of changing U, L and AOA in real flow field.

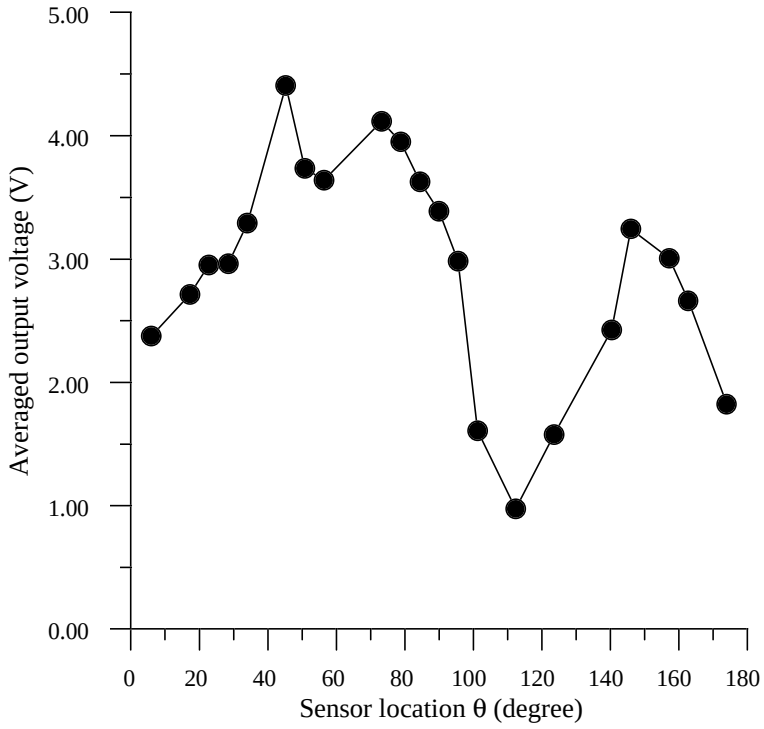

Figure 6.16 Averaged output from one row of sensors on a skin.

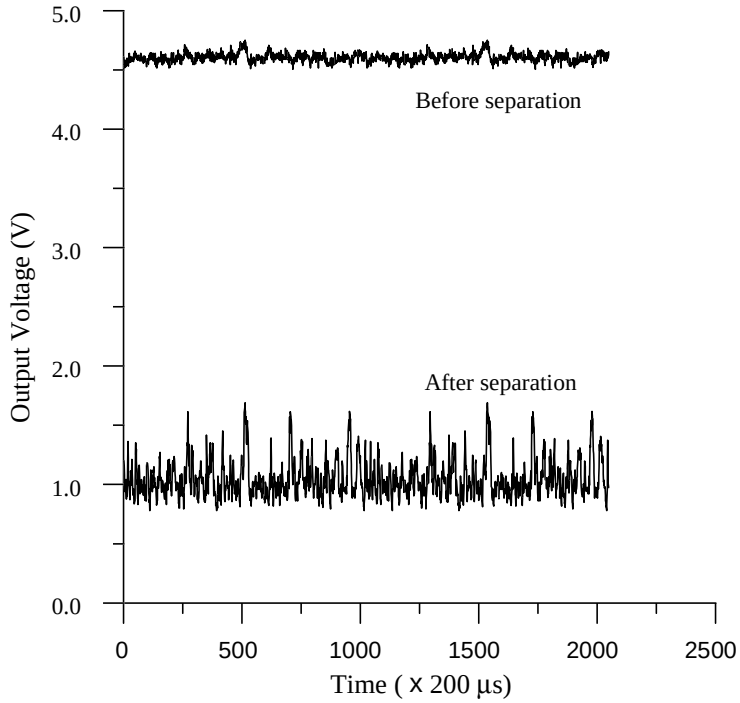

Figure 6.17 Output voltages (after gain of 10) from the sensors located before and after the flow separation point at velocity of 30 m/s.

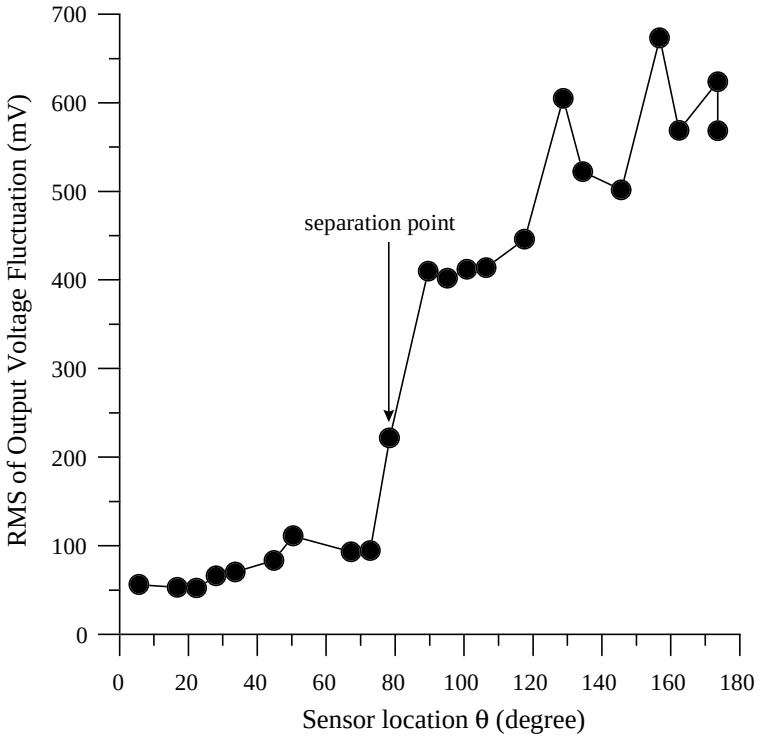

Figure 6.18 RMS fluctuation used to identify separation point.

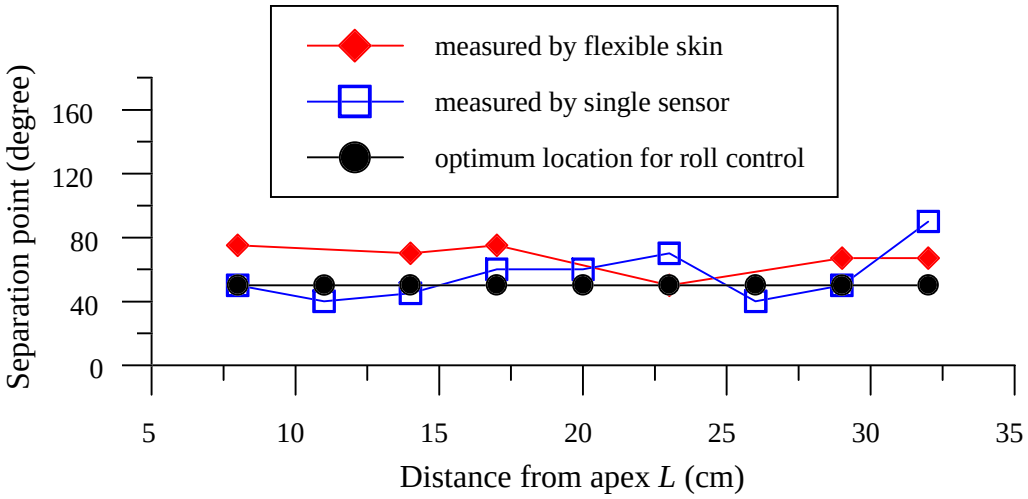

Figure 6.19 Comparison of separation lines measured by a single sensor and a flexible shear stress sensor array.

6.6 Sensor-Actuators Skin and Conformable M^3 System

The flexible MEMS technology has been applied to the fabrication of sensor-actuator skins. The sensors are the shear stress sensors and the actuators are the surface micromachined magnetic coil flap previously developed by the Caltech Micromachining Lab [20]. Figure 6.20 shows the layout of the sensor and actuator arrays on the 1×3 cm^2 skin. It has 1×36 sensors and 3×9 actuators. The purpose of the skin with this layout design is for the real-time control of the delta wing model in UCLA.

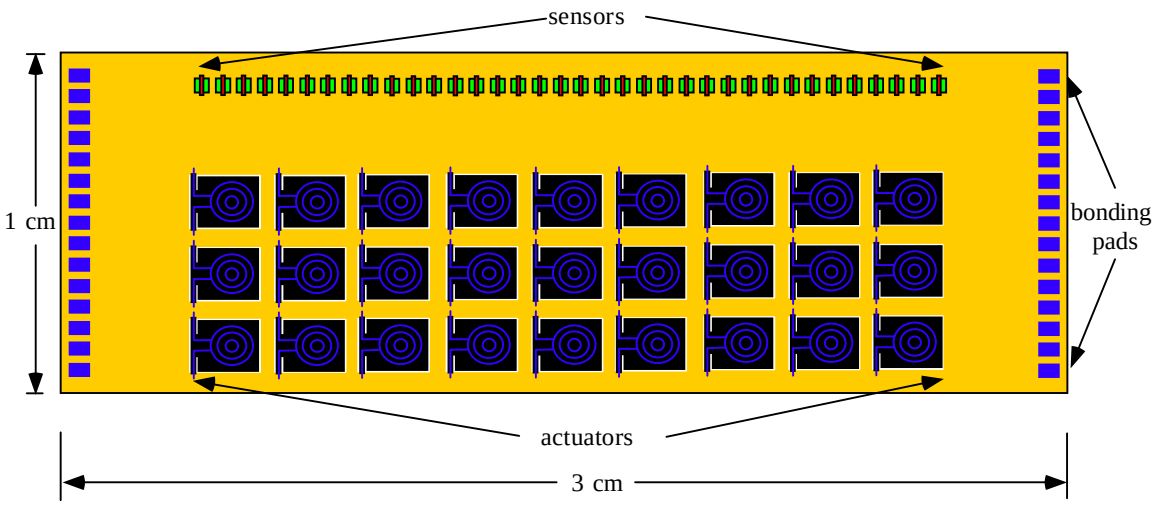

Figure 6.20 Layout design of the sensor-actuator skin for delta wing control.

Figure 6.21 the simplified fabrication process flow. Here, thick (2 μm) thermal silicon dioxide, instead of aluminum, is used as the etch stop in the final RIE etch step because aluminum can not be deposited under the flaps. This small change has actually caused some major problems. First, since the thermal oxide is grown on most of the front side but not on the backside, the wafer warpage caused by its intrinsic stress after the Si diapgram is formed becomes very serious. The solution is to grow thermal oxide on the backside. Second, as soon as the silicon under the flap area is removed by the final RIE etching, the flaps curl so badly due to the huge intrinsic stress that many of their torsional beams are broken. Figure 6.22 shown the sensor-actuator skin with the highest flap survival rate (80%) on a wafer. The solution is to spin-coat a few microns of polyimide

on the front side and bake the wafer at 150^{o}C for 30 min. before the RIE etching. The flaps are then protected against curling by the polyimide during and after the RIE etching. By first etching away the exposed oxide with BHF and then removing the protective polyimide with acetone/alcohol, the flaps are free-standing. However, even the surface flaps can survive the process, they are usually not robust in flow field and not very effective in flow control. The bulk flap is probably the better choice.

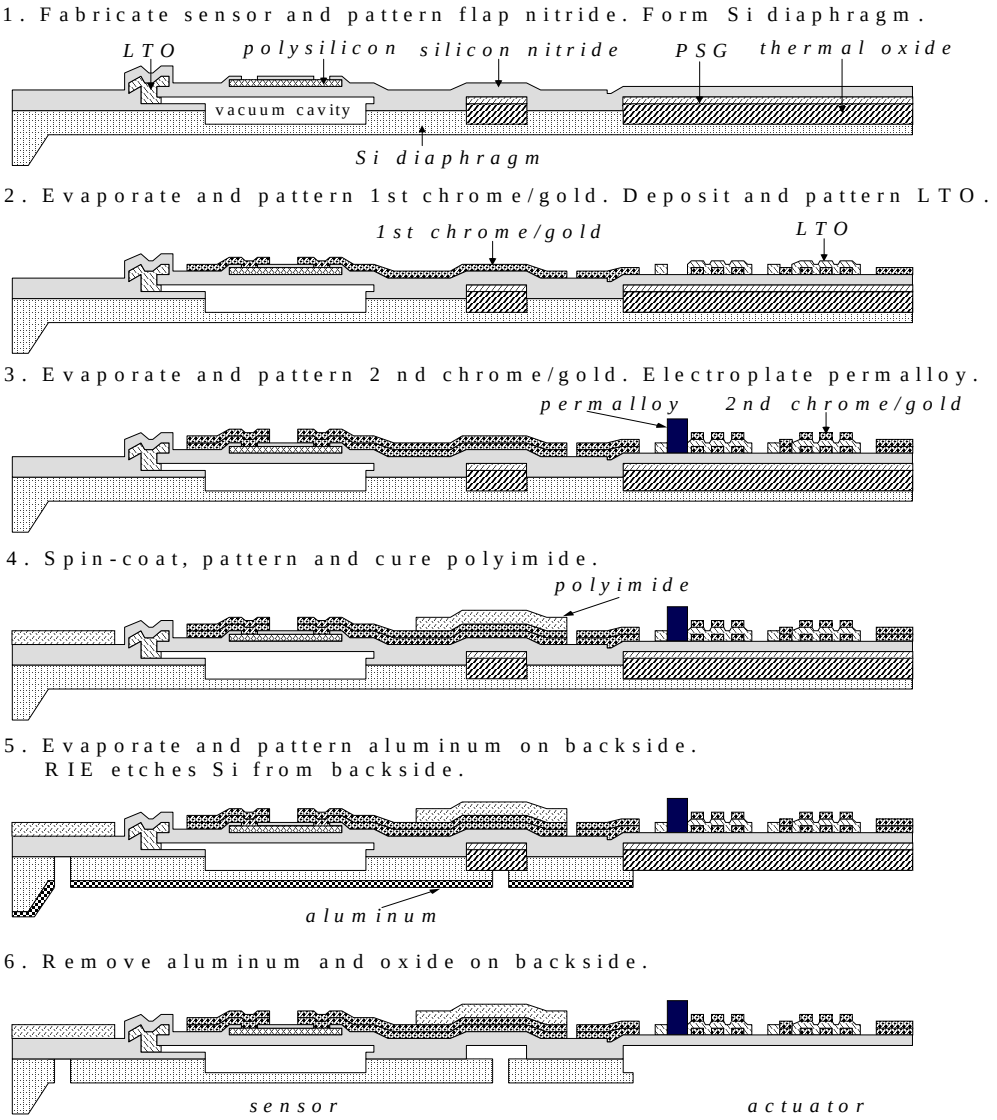

Figure 6.21 Simplified process flow for the sensor-actuator skin.

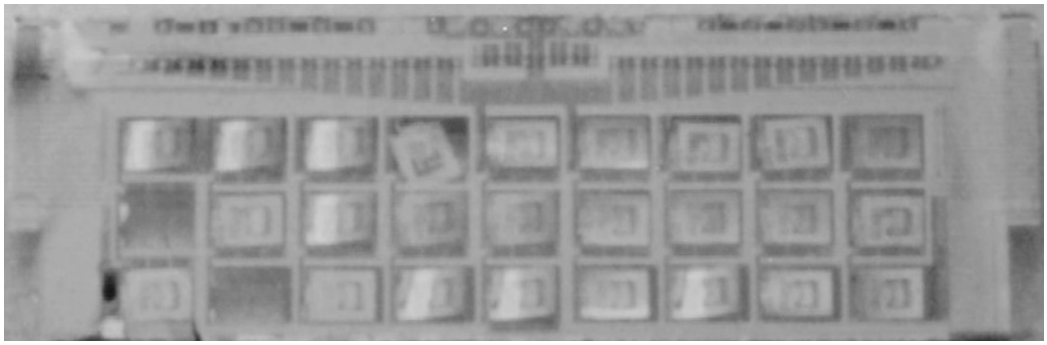

Figure 6.22 Picture of the best sensor-actuator skin on a wafer.

Finally, we propose the conformable M^3 system for delta wing control. Its cross-section is shown in Figure 6.23, which is basically the flexible skin version of the M^3 system for drag reduction described in Chapter 5. Here we have chosen the bulk micromachined flaps as the micro-actuators. The first polyimide layer serves as the inter-metal insulation for the flaps as well as the part of the flexible skin. It can be replaced by PSG or other inter-metal insulation materials with only a minor sacrifice on the robustness of the skin if it is not used by the IC manufacturers.

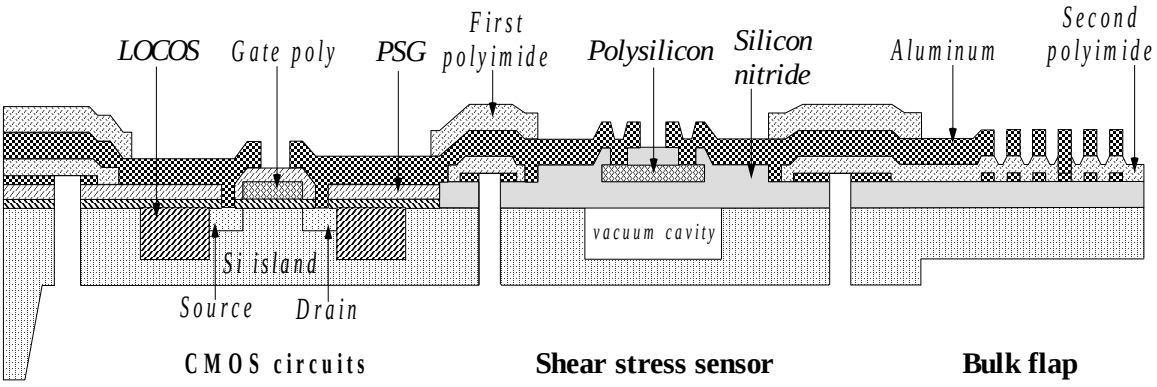

Figure 6.23 Cross-section of the proposed conformable M^3 system for delta wing control.

6.7 Summary

A novel flexible MEMS skin technology has been developed and it is fully compatible with IC process. The major lead failure occurred in previously reported technologies has been eliminated through the proper shaping of Si islands. Moreover, Si

islands as small as 100 μm can be defined with good accuracy, which allows the skins to be applied on small surfaces with large curvatures. The first application of this technology has produced a flexible shear stress sensor array that was successfully used in aerodynamics for the real-time measurement of shear stress distribution on 3-D surfaces.

Bibliography

[1] F. Jiang, Y.C. Tai, B. Gupta, R. Goodman, S. Tung, J.B. Huang, and C.H. Ho, "A Micromachined Shear Stress Sensor Array," *Proc. IEEE MEMS-96 Workshop*, San Diego, pp. 110-115, 1996.

[2] P.W. Barth, S. L. Bernard, and J. B. Angell, "Flexible Circuit and Sensor Arrays Fabricated by Monolithic Silicon Technology," *IEEE Trans. Electron. Devices*, Vol. ED-32 (7), pp. 1202-1205, 1985.

[3] D. J. Beebe and D. D. Denton, "A Flexible Polyimide-Based Package for Silicon Sensors," *Sensors and Actuators*, Vol. A44, pp. 57-64, 1994.

[4] C. Bang and T. Pan, "Flexible Heat Flux Sensor Arrays," *AFOSR Contractor and Grantee Meeting on Turbulence and Internal Flows*, Atlanta, Georgia, Sept. 1996.

[5] M. Mehregany, R. G. DeAnna, and E. Reshotko, "Microelectromechanical Systems for Aerodynamics Applications," AIAA Paper 96-0421, 1996.

[6] W. J. McCroskey and E. J. Durbin, "Flow Angle and Shear Stress Measurements using Heated Films and Wires," *ASME J. Basic Engineering*, Vol., pp. 46-52, 1972.

[7] H. H. Bruun, *Hot-Wire Anemometry: Principles and Signal Analysis*, Oxford University Press, p. 276, 1995.

[8] D. C. Reda, "Rise-Time Response of Nickel-Foil-on Kapton-Substrate, Hot-Film, Shear-Stress Sensors," AIAA Paper 91-0169, 1991.

[9] M. S. Wusk, D. L. Carraway, and B. J. Holmes, "An Arrayed Hot-Film Sensor for Detection of Laminar Boundary-Layer Flow Disturbance Spatial Characteristics," AIAA Paper 88-4677, 1988.

[10] J. P. Stack, S. M. Mangalam, and S. A. Berry, "A Unique Measurement Technique to Study Laminar-Separation Bubble Characteristics," AIAA Paper 87-1271, 1987.

[11] J. P. Stack, S. M. Mangalam, and V. Kalburgi, "The Phase Reversal Phenomenon at Flow Separation and Reattachment," AIAA Paper 88-0408, 1088.

[12] DuPont Electronic Materials, *PI-2808 Polyimide Product Information*, 1994.

[13] DuPont, *Kapton Polyimide film Productor Information*.

[14] B. Gupta, R. Goodman, F. Jiang, Y. C. Tai, S. Tung, and C. H. Ho, "Analog VLSI System for Active Drag Reduction," *IEEE Micro*, Vol. 16, No. 5, pp. 53-59, 1996.

[15] B. J. Bellhouse and D. L. Schultz, "Determination of Mean and Dynamic Skin Friction, Separation and Transition in Low-Speed Flow with a Thin-Film Heated Element," *J. Fluid Mech.*, Vol. 24, part 2, pp. 379-400, 1966.

[16] E. Achenbach, "Total and Local Heat Transfer from a Smooth Circular Cylinder in Cross-Flow at High Reynolds Number," *Int. J. Heat & Mass Transfer*, Vol. 18, pp.1387-1396, 1975.

[17] C. Liu, T. Tsao, Y. C. Tai, J. Leu, and C. H. Ho, "Out-of-Plane Permalloy Magnetic Actuators for Delta-Wing Control," *Proc. IEEE MEMS'95*, pp. 328-331, 1995.

[18] G. B. Lee, F. Jiang, T. Tsao, Y. C. Tai, and C. M. Ho, "Macro Aerodynamic Devices Controlled by Micro Systems," *IEEE Aerospace Conference*, Snowmass, Colorado, 1997.

[19] G. B. Lee, C. M. Ho, F. Jiang, C. Liu, T. Tsao and Y. C. Tai, "Distributed Flow Control by MEMS," *ASME 1996 International Mechanical Engineering Congress and Exposition*, Atlanta, Nov. 17-22, 1996.

[20] T. Tsao, F. Jiang, R. Miller, Y. C. Tai, B. Gupta, R. Goodman, S. Tung, and C. H. Ho, "An Integrated MEMS System for Turbulent Boundary Layer Control," *Transducers'97*, Chicago, pp. 315-318, 1997.